Research Article

TiO$_2$/Diazonium/Graphene Oxide Composites: Synthesis and Visible-Light-Driven Photocatalytic Degradation of Methylene Blue

Nguyen Thi Vuong Hoan (iD),[1] **Nguyen Ngoc Minh**,[1] **Thoi Thi Kim Nhi**,[1] **Nguyen Van Thang**,[1] **Vu Anh Tuan** (iD),[2] **Vo Thang Nguyen**,[3] **Nguyen Mau Thanh**,[4] **Nguyen Van Hung** (iD),[5] **and Dinh Quang Khieu** (iD)[6]

[1]*Quy Nhon University, 590000, Vietnam*
[2]*Institute of Chemistry, Vietnam Academy of Science and Technology, 100000, Vietnam*
[3]*University of Education and Science, The University of Da Nang, 550000, Vietnam*
[4]*Falculty of Natural Sciences, Quang Binh University, 510000, Vietnam*
[5]*Center for Chemistry Analysis, Dong Thap University, 870000, Vietnam*
[6]*University of Sciences, Hue University, 530000, Vietnam*

Correspondence should be addressed to Nguyen Thi Vuong Hoan; nguyenthivuonghoan@qnu.edu.vn, Nguyen Van Hung; nguyenvanhung@dthu.edu.vn, and Dinh Quang Khieu; dqkhieu@hueuni.edu.vn

In the present article, the synthesis of TiO$_2$/diazonium/graphene oxide and its photocatalytic activity for methylene blue (MB) degradation have been demonstrated. The functionalization of graphene oxide (GO) with diazonium salt (diazonium-GO) was conducted for enhancing the dispersibility of GO in distilled water. TiO$_2$ was highly dispersed in diazonium-GO to form TiO$_2$/diazonium/graphene. The obtained specimens were characterized by X-ray diffraction, FT-IR spectroscopy, Raman spectroscopy, UV-Vis spectroscopy, scanning electron microscope, transmission electron microscopy, and X-ray photoelectron spectroscopy. It was found that the TiO$_2$ phase in TiO$_2$/diazonium/GO composites can be controlled by adjusting the amount of ethanol or titanium oxide in the reactant mixture. The obtained composites exhibited photocatalytic activities for methylene blue degradation (MB). The composite with *ac.* 70% anatase can provide the highest MB degradation efficiency. The studying of some intermediates for MB photocatalytic degradation using LC-MS showed that structure of MB by the cleavage and oxidation of one or more of the methyl group substituent on the amine groups lead to form compounds with low molecular masses. Total organic carbon studies confirmed a complete mineralization of MB. The present catalyst was stable and recyclable after three times with a negligible loss of catalytic activity. In addition, the TiO$_2$/diazonium/GO can also photocatalyze for the degradation of some other dyes (phenol, methyl red, and Congo red).

1. Introduction

Titanium oxide-based materials in several types and forms have exhibited excellent potential as powerful photocatalysts for various reactions thanks to their chemical stability, non-toxicity, and high reactivity and interesting materials with nonline optical properties for applications in ultrafast optical information processing, optical switching, and optical limiting for protection against strong laser radiation [1]. In particular, titanium oxide has been used for such significant applications as the solar photons for the photocatalytic depollution [2], energy conversion [3], and purification of polluted water and air [4]. It is well known that three polymorphs of titania are brokite, anatase, and rutile. Rutile is a

stable phase while brokite and anatase are metaphases. Because of the difficulty in the synthesis, the catalytic activity of brokite is seldom reported. Anatase exhibits higher catalytic activities compared with those of rutile [5, 6]. However, detailed mechanisms and factors influencing different activities of these polymorphs are controversial. During the photocatalytic process, the photo-induced electrons and holes are generated because the electrons are excited from the valence band (VB) of TiO_2 to the conduction band (CB). The holes and electrons will react with water and oxygen to form free radicals which can oxidize and decompose the organic compounds [7]. However, the fast recombination of excited state CB electrons and VB holes without initiating the photocatalytic activity limits TiO_2 in catalytic applications. Many approaches of preventing the photo-induced electron-hole recombination have been reported, such as using TiO_2 composites with transition metal oxides [8, 9], noble metals [10, 11], and carbon nanotubes (CNT) [12, 13].

Graphene is an interesting material because of its unique electronic property [14], high mobility and transparency [15], flexible structure, and high surface area [16]. Graphene oxide (GO) could be considered as graphene functionalized by hydroxyl, carboxylic acid, and epoxide groups [17, 18], and their properties are sensitive to chemical doping, adsorbed or bound species [19]. Generally, an electron energy gap could be varied by oxidation of graphene, and the value of the energy gap depends on oxidization degree of graphene and species of oxygen-containing groups. It means that GO could change from conducting to insulating by tuning the C/O ratios [20, 21].

The combination of TiO_2 with GO is considered as the versatile composite for photocatalyst due to the excellent absorbability and conductivity of GO. Much attempt on investigation into the synthesis and application of TiO_2/GO composites as photocatalyst has been reported. Chen et al. [22] reported the synthesis of visible-light-driven graphene oxide/TiO_2 composites with p/n heterojunction from $TiCl_3$ source, and these semiconductors could be excited by visible light and acted as a sensitizer in graphene oxide/TiO_2 composites. TiO_2 nanorods are self-assembled on the graphene oxide sheets at the water/toluene interface [23]. During the preparation of GO–TiO_2 composites by sonicating the dispersed TiO_2 nanoparticles and GO in ethanol, Williams et al. [24] found that GO can be reduced photocatalytically by TiO_2 under UV light irradiation. However, the formation of homogeneous mixture of TiO_2 and GO is often a problem because the easy formation of agglomeration of both titania and GO prevents the effective dispersion of these metal oxide nanoparticles in a GO matrix. In order to overcome this experimental hinderance, several GO derivatives have been prepared by grafting new functional groups such as ethylenediamine [25], EDTA [26], and diazonium of sulfanilic acid [27] through a GO backbone to form the water soluble GO; as a result, nanooxide particles are effectively dispersed in a GO matrix. Continuing this idea, in the present paper, GO was modified by the diazonium salt of sulfanilic acid prior to dispersion of TiO_2 on GO with

an idea to enhancing the possibility of inserting active oxygen-containing polarization groups between graphite layer in graphene oxide, which adjusts the semiconductivity of graphene oxide in the obtained composite. The photocatalytic activity of the TiO_2/diazonium/GO composite material was evaluated by the degradation of methylene blue (MB) in the visible light region.

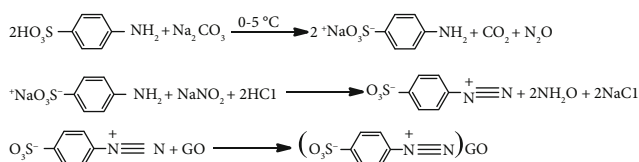## 2. Experimental

2.1. Materials. Graphite powder (C, 99%), titanium tetrachloride ($TiCl_4$, 99%), potassium permanganate ($KMnO_4$, 99.5%), sodium nitrate ($NaNO_3$, 99%), sulfuric acid (H_2SO_4, 98%), and ethanol (C_2H_5OH, 99.5%) were purchased from Merck. Hydrogen peroxide (H_2O_2, 30%), sulfanilic acid (($H_2N)C_6H_4SO_3H$, 99.8%), ammonia solution (NH_4OH, 25%), hydrochloric acid (HCl, 37%), 1,4-benzoquinone ($C_6H_4O_2$, ≥99%, BQ), dimethyl sulfoxide (($CH_3)_2SO$, 99.9%, DMSO), diamonium oxalate (($NH_4)_2C_2O_4·H_2O$), ≥99.5%, AO), *tert*-Butanol (($CH_3)_3COH$, ≥99%, TB), and methylene blue ($C_{16}H_{18}N_3SCl$, MB) were obtained from Sigma-Aldrich. All chemicals used were of analytical grade and were used as received without any further purification.

2.2. Synthesis of Graphene Oxide. GO was synthesized by a modified Hummers' method [28]. In a typical synthesis, 1.0 g of graphite powder was added into 2.5 g of $NaNO_3$ and 100 mL of concentrated H_2SO_4 under magnetic stirring. Then, 3.0 g of $KMnO_4$ was slowly added to this mixture at 10°C under stirring for 2 h before adding 100 mL of distilled water and heating up to 98°C under stirring for another 2 h. After that, 10 mL of H_2O_2 was poured into the mixture with stirring for 2 h. As the result, the color of the mixture changed to bright yellow. Finally, the mixture was filtered and washed with a 5% HCl aqueous solution to remove metal ions, followed by distilled water for removal of the acid. The brown-black solid obtained was separated by ultrasonic treatment in water and then dried at 60°C for 12 h.

2.3. Synthesis of TiO_2/Diazonium/GO Composites. The preparation of modified graphene oxide was carried out as follows. Firstly, the diazonium salt was prepared by dissolving 46 mg of sulfanilic acid in 10 mL of distilled water containing 30 mg of Na_2CO_3 in ice bath, then heating gently for sulfanilic acid to dissolve completely [27]. Next, 18 mg of $NaNO_2$ was dissolved into 5 mL of distilled water before being added to the prepared sulfanilic acid solution. A 1 N HCl solution (2.4 mL) was added dropwise to the above mixture and stirred to obtain diazotized sulfanilic acid. Next, 75 mg of GO was added to the diazonium solution and stirred continuously for 2 hours. The solid was separated by filtering and drying. The samples were diazotized sulfanilic acid-GO (denoted as Dia-GO). Sulfanilic acid contains a sulfo group (SO_3H) and an amino group (NH_2). The amino group can react with cold nitrous acid to produce diazotized sulfanilic acid which can be used to synthesize the sulfonated graphene oxide composite.

The reactions are assumed as follows:

$$2HO_3S - \bigodot - NH_2 + Na_2CO_3 \xrightarrow{0\text{-}5\,°C} 2 \, ^+NaO_3S - \bigodot - NH_2 + CO_2 + N_2O$$

$$^+NaO_3S - \bigodot - NH_2 + NaNO_2 + 2HCl \longrightarrow O_3S^- - \bigodot - \overset{+}{N} \equiv N + 2NH_2O + 2NaCl$$

$$O_3S^- - \bigodot - \overset{+}{N} \equiv N + GO \longrightarrow \left(O_3S^- - \bigodot - \overset{+}{N} \equiv N \right) GO$$

The composite of TiO_2/Dia-GO was prepared as described elsewhere [29]. Firstly, the effect of $TiCl_4$ concentration on the phase formation of TiO_2 phases was studied. 15 mg of Dia-GO was dissolved in 120 mL solvent (40 mL ethanol/80 mL distilled water) under ultrasonication for 2 hours. The mixture was cooled down at 0-5°C. Then, 2 mL $TiCl_4$ was added slowly at different concentration to Dia-GO suspension under vigorous stirring to obtain the brown suspension. The resulting suspension was added to an autoclave at 180°C for 12 hours. The obtained solid was separated by filter and washed by distilled water for several times and then dried at 60°C for 6 hours. The obtained samples are denoted as Tx-y/Dia-GO: T0.05-40/Dia-GO, T0.15-40/Dia-GO, T0.45-40/Dia-GO, and T1.35-40/Dia-GO with the symbol of $x = 0.05$, 0.15, 0.45, and 1.35 representing the concentration in mole of titanium chloride and y of 40 representing the mL ethanol in 120 mL mixture. Subsequently, the effect of ethanol/water ratio (v/v) used for the hydrolysis on the titania phases was investigated. The procedure was similar to the one mentioned above but only 120 mL mixture with the amount of ethanol differed from 20 to 120 mL. The sample as denoted as T0.05-20/Dia-GO, T0.05-40/Dia-GO, T0.05-60/Dia-GO, T0.05-80/Dia-GO, T0.05-100/Dia-GO, and T0.05-120/Dia-GO corresponding to the ethanol/distilled water (v/v) being 20/100, 40/80, 60/60, 80/40, 100/20, and 120/0.

2.4. Characterization of Materials. The X-ray diffraction (XRD) data of all samples were collected in a D8 Advanced Bruker anode X-ray Diffractometer with Cu Kα. The quantitative analysis of mixture of anatase-rutile was performed using the XRD method as previously proposed [30]. Particle diameters smaller 5 microns are desirable to ensure adequate reproducibility of diffraction intensity measurement.

$$X_R = \frac{1}{1 + 0.8(I_A/I_R)} \cdot 100\%,$$

$$X_A = \frac{1}{1 + 1.26(I_R/I_A)} \cdot 100\%, \tag{1}$$

where I_A and I_B, respectively, are the intensity of diffraction at (110) for rutile phase and (101) for anatase phase; X_R and X_A are the percentage of rutile and anatase, respectively; the experimental parameters of 0.80 and 1.26 are obtained from the regression of the relative given amount of anatase and rutile versus I_R/I_A.

Transmission electron microscope (TEM) images were obtained by JEOL JEM-2100F. FT-Infrared (IR) spectra for
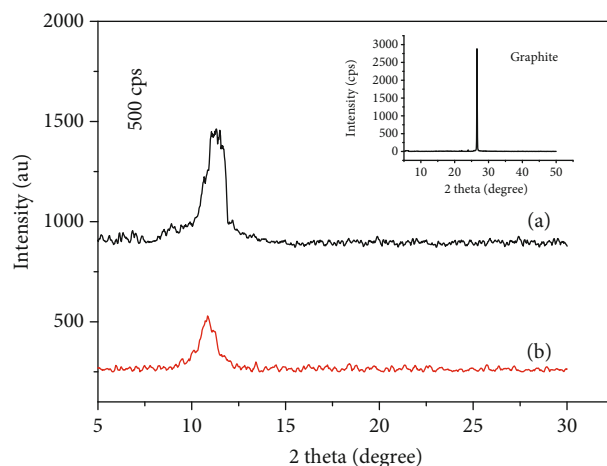

FIGURE 1: X-ray diffraction patterns for GO (a), Dia-GO (b), and the inset present the XRD pattern of graphite.

the samples were recorded on an IR Prestige-21 spectrophotometer (Shimadzu). X-ray photoelectron spectrometry (XPS) was used for surface analysis with an ESCALAB 250 (Thermo VG, UK) spectrometer with X-ray source monochromated Al Kα radiation (1486.6 eV). DRS-UV-Vis spectra were recorded with Jasco-V670 instrument. The measurement of photoluminescence (PL) was conducted by means of a spectrometer Horiba Jobin-Yvon HR800 LabRam using UV excitation. The identification of MB degradation was performed using a liquid chromatography-mass spectrometry (LC-MS) method (Ultimate 3000 plus, Hypersil GOLD C18 (150×2.1 mm, $2.0\,\mu$m), Thermo, MA, USA).

2.5. Photocatalytic Activity. In this study, the photocatalytic activities of obtained materials were investigated via the degradation of methylene blue (MB) in an aqueous solution under the irradiation of 75 W-220 V filament lamps (Dien Quang) with a UV cut off filter ($\lambda < 390$ nm, $d = 77$ mm).

The experiments were carried out with a 500 mL dye solution at various concentrations containing 100 mg of catalyst. The mixture was stirred continuously for 2 hours in the dark to establish an adsorption-desorption equilibrium before turning on the lamp. Three millites of solution were withdrawn after a certain time and centrifuged to remove the solid. The concentration of MB in solution was determined by its absorption at λ max = 664 nm. Each experiment was in triplicate.

The performance of MB mineralization was calculated based on TOC (total organic carbon) measurements from

$$M = 100 \times \frac{TOC_0 - TOC_t}{TOC_0}, \tag{2}$$

where TOC_0 and TOC_t are the MB concentrations at the initial and time t of the reaction, respectively. The concentration of TOC was determined using a TOC analyzer (model: Multi N/C®2100 S, Analytik Jena, Germany).
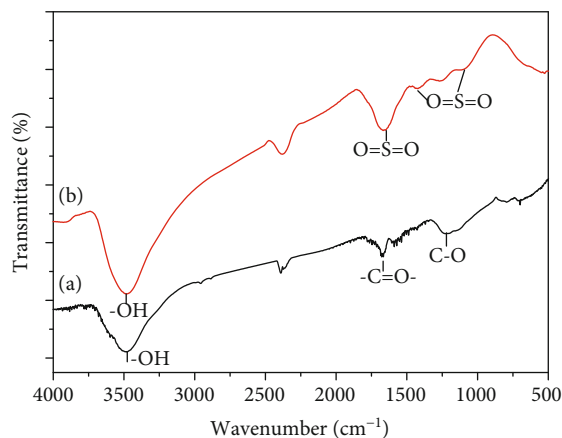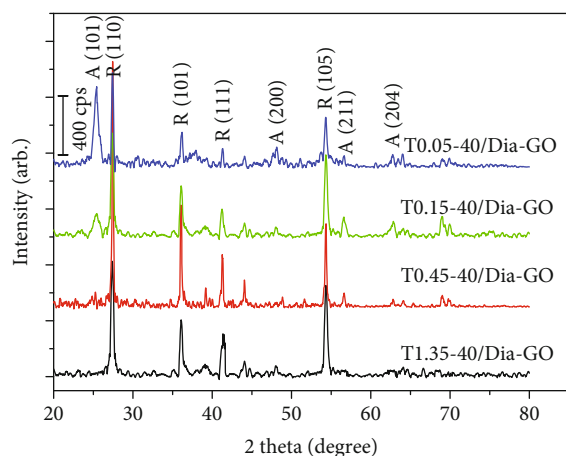
FIGURE 2: FTIR spectra of GO (a), Dia-GO (b).
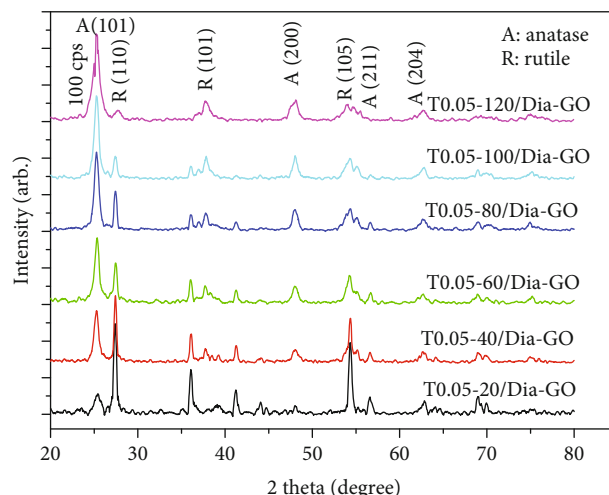

FIGURE 3: XRD patterns of TiO$_2$/Dia-GO samples.

FIGURE 4: X-ray diffraction patterns for T0.05-y/Dia-GO samples (y = 20, 40, 60, 80, 100, and 120 mL ethanol).

TABLE 1: Phase composition and methylene blue conversion (%) of TiO$_2$/Dia-GO composites ($C_{0,MB}$ = 100 mg/L, V = 100 mL, m_{Cat} = 100 mg, and time = 120 min).

Notation	Phase composition (%)		MB conversion (%)
	Anatase	Rutile	
T1.35-40/Dia-GO	0	100	23.41
T0.45-40/Dia-GO	0	100	24.84
T0.15-40/Dia-GO	15.25	84.75	45.28
T0.05-40/Dia-GO	40.25	59.75	48.73
T0.05-60/Dia-GO	58.89	41.11	54.23
T0.05-80/Dia-GO	62.19	37.81	57.05
T0.05-100/Dia-GO	73.45	26.55	69.82
T0.05-120/Dia-GO	100	0	63.55

3. Results and Discussion

3.1. Characterization of Materials

3.1.1. Preparation of Diazonium/GO (Dia-GO).
Figure 1 presents XRD patterns of graphite, GO, and Dia-GO. The sharp peak around 26.5° is characteristic of graphite [31] (the inset of Figure 1). The peak at around 11.4° of GO can be attributed to the introduction of oxygen-containing functional groups into the graphite sheets to form of graphene oxide [32]. These functional groups, especially the -SO$_3$H group between the layers of GO, interact strongly with polarizing groups on GO, leading to a shift of a 2θ angle to the smaller value in GO [33, 34], resulting in an increase in $d_{spacing}$ from 7.82 Å for GO to 8.11 Å for Dia-GO (Figures 1(a) and 1(b)). The similar results have been also obtained in the reported papers [34–36] in which GO is chemically functionalized with diazonium of sulfanilic acid.

From Figure 2, it can be seen that the GO shows characteristic bands of oxygen-containing functional group vibrations: hydroxyl group (-OH) over the range of 3400-3500 cm^{-1}, C=O vibration (-COOH) at 1636-1700 cm^{-1}, and C-O vibration at 1229 cm^{-1} and 1060 cm^{-1} [37–39]. In addition, there are also characteristic peaks for the oscillation of

the O=S=O (group -SO$_3$H) bond at 1620-1650 cm^{-1}, 1400 cm^{-1}, and 1100 cm^{-1} [40–43] in Dia-GO. These results confirmed the formation of diazonium/graphene oxide.

3.1.2. The Preparation of TiO$_2$/Diazonium/GO.
The effect of TiCl$_4$ concentration on the phase formation of TiO$_2$ was investigated by XRD studies (Figure 3).

It can be seen that the obtained samples all exhibit characteristic diffraction peaks of titanium oxide. As seen in Figure 3, the formation of titanium oxide phases (rutile or anatase) depended on titanium chloride concentration. The rutile phase was formed primarily as the titanium chloride concentration was high. T1.35-40/Dia-GO composed of mainly rutile phase with characteristic peaks at 2θ angles of 27.4°, 36.1°, and 41.3° indexed as (110), (101), and (111), respectively (JCPDS: No 21-1276), whereas anatase phase increased with a decrease in titanium chloride concentration. The characteristic peaks with increasing intensity of anatase phase were observed at angles 2θ of 25.5°, 37°, 53.9°, 56.5°, and 62.5° indexed as (101), (004), (200), (105), and (211), respectively (JCPDS: No 21-1272). Primary estimation of
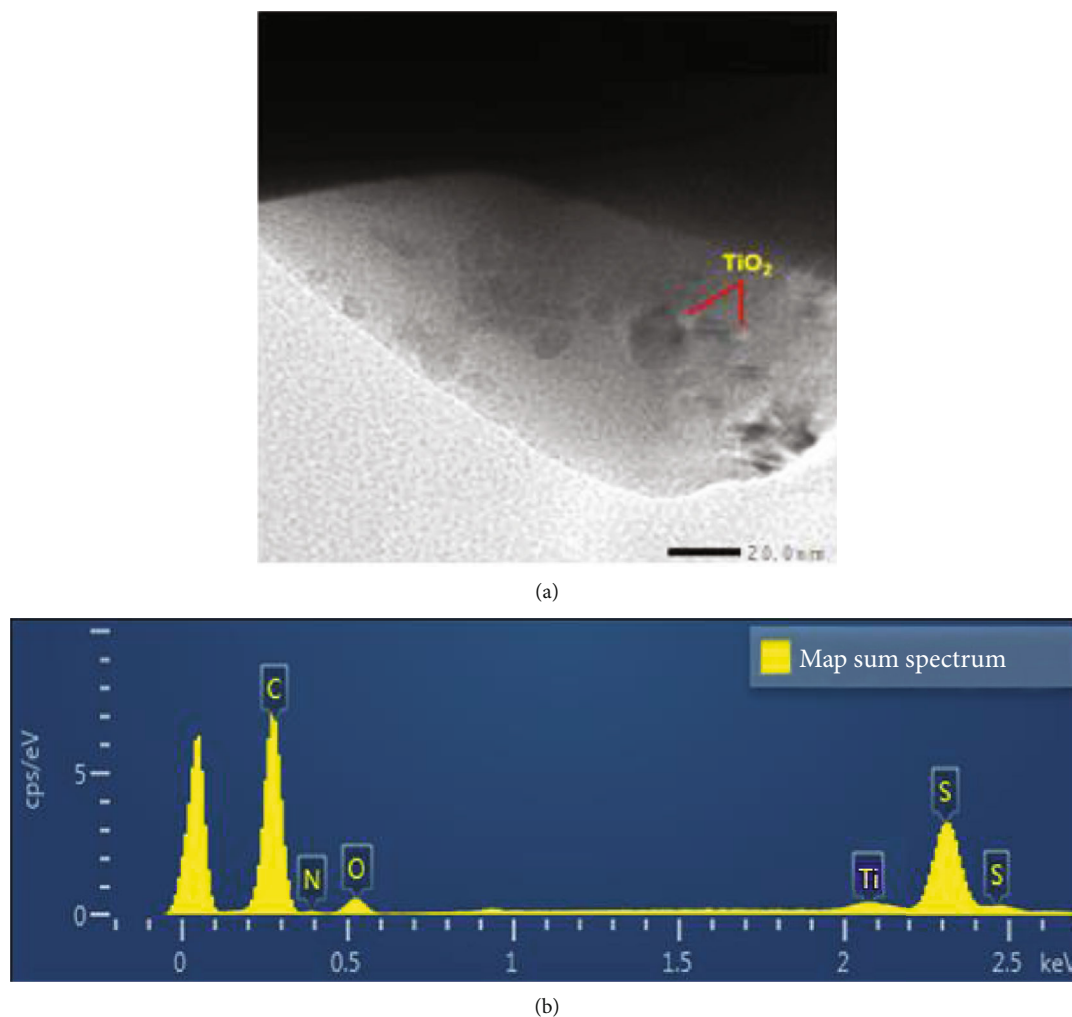
(a)

(b)

FIGURE 5: (a) TEM observation and (b) EDX spectrum of T0.05-100/Dia-GO.
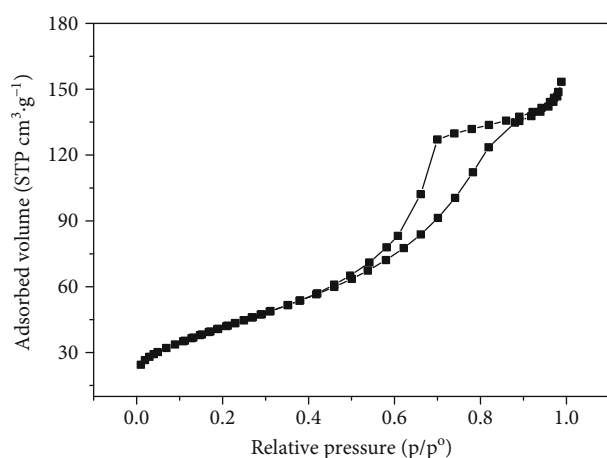

FIGURE 6: The nitrogen adsorption/desorption isotherms of T0.05-100/Dia-GO.

catalytic activity for the obtained composite revealed that the use of T0.05-40/Dia-GO led to the highest yield of MB degradation. Therefore, T0.05-40/Dia-GO was selected to further

study the effect of ethanol/distilled water ratio on the formation of titanium oxide.

The composition of titanium oxide depends not only on titanium chloride concentration but also on the amount of ethanol used in the hydrolysis step. Figure 4 shows XRD patterns of T0.05-y/Dia-GO composite materials synthesized at various amounts of ethanol y (y: 20-120 mL of ethanol used).

For T0.05-120/Dia-GO, TiO_2 phase existed mainly in anatase form with the characteristic diffraction peaks at 2θ angle of 25.5° with high intensity. The intensity of this characteristic peak decreased with the decrease of ethanol/distilled water ratio. Meanwhile, the intensity of characteristic diffractions at 27.4° and 36.1° for rutile increased significantly with the decrease of the ethanol/distilled ratio. The quantitative analysis of titanium oxide phase showed that when the amount of ethanol increased from 20 mL to 120 mL, the anatase TiO_2 phase composition increased from 15.25% to 100%, corresponding to the reduction of rutile phase composition from 84.75% to 0%. Thus, in the samples of synthetic materials, titanium oxide existed in both forms, anatase and rutile.

The results of photocatalytic activity of TiO_2/Dia-GO nanocomposite are listed in Table 1. It can be seen that
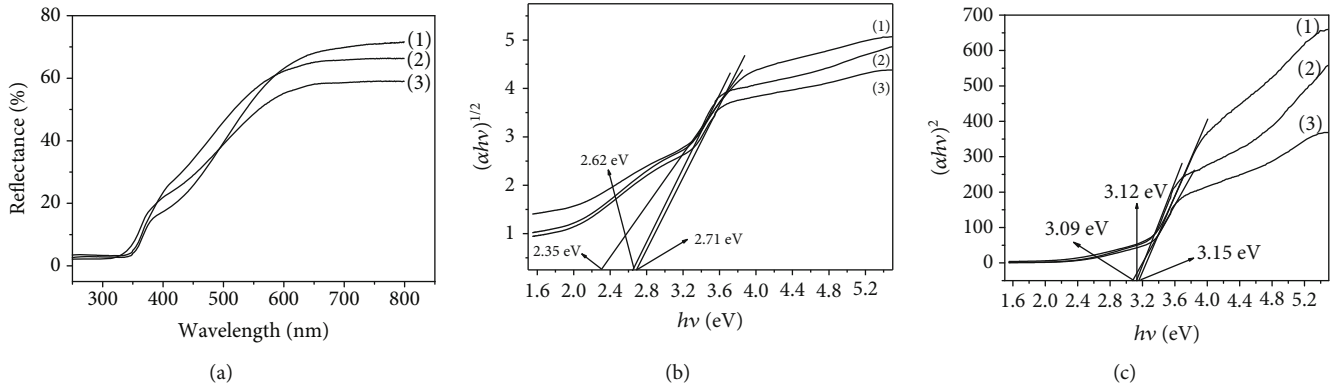
FIGURE 7: (a) DRS-UV-Vis spectra of TiO$_2$/GO (1), Dia-GO (2), and T0.05-100/Dia-GO (3); (b) Tauc's plots of $(\alpha h\nu)^{1/2}$ vs. $h\nu$ and (c) of $(\alpha h\nu)^2$ vs. hν for TiO$_2$/GO (1), Dia-GO (2), and T0.05-100/Dia-GO (3).

TABLE 2: E_g values for direct and indirect transitions of the investigated samples.

Sample	E_g (indirect) (eV)	E_g (direct) (eV)
TiO$_2$/GO	2.71	3.15
Dia-GO	2.62	3.12
T0.05-100/Dia-GO	2.35	3.09

photocatalytic activity depended significantly on titania phase composition. Composite with 100% TiO$_2$ in rutile phase exhibited the lowest photocatalytic activity on MB degradation (around 23.4%). The photocatalytic activity increased with an increase in the amount of anatase phase. The MB degradation efficiency peaked at 69.8% as the anatase phase growed to around 73.4% (corresponding to T0.05-100/Dia-GO) before slightly reducing when the amount of anatase phase kept increasing. It is well-known that anatase has lower absorbance ability towards visible light than rutile due to the larger band gap (3.2 eV) than that (3.0 eV) of rutile. However, its indirect band gap provides a longer lifetime of photoinduced electron/hole pairs than direct band gap in rutile because the direct recombination of photoexcited electrons from the conduction band to valence band of anatase TiO$_2$ is impossible [6]. The mixture with an appropriate ratio of anatase and rutile should provide the more superior photocatalytic activity than that of individual rutile or anatase. Then, T0.05-100/Dia-GO was selected for further experiments.

The morphologies of T0.05-100/Dia-GO observed by TEM are shown in Figure 5. The TiO$_2$ nanoparticles were dispersed highly over the Dia-GO sheet with an average particle size of 5-15 nm (Figure 5(a)). The crystallite size of 11.7 nm obtained by Debye-Scherrer analysis at (101) diffraction is close to the average size of TiO$_2$ particles observed by TEM indicated that the morphology of T0.05-100/Dia-GO consists of single crystals of TiO$_2$ highly dispersed on Dia-GO. Elemental analysis for composite surface showed that T0.05-100/Dia-GO consisted of N, S, and Ti (Figure 5(b)) as an additional evidence of the successful synthesis of the composite of TiO$_2$/diazonium/GO.

Based on the band theory of semiconductors, the conduction band (CB) of TiO$_2$ is mainly determined by the Ti 3d orbital energy levels, while the valence band (VB) is mainly formed from the O2p orbitals. As compared to the O2p orbital, other nonmetal elements such as N and S, P possess 2p orbitals locating at more negative energy levels; hence, the partial substitution of the impurity dopants N and S will result in the formation of new energy bands above the TiO$_2$ valence band, thus providing the photocatalytic activity over the visible light region of TiO$_2$ [44].

The textural property of the obtained composite was estimated by means of the nitrogen adsorption/desorption isotherms (Figure 6). The isotherm curve is the type IV and H3 according to IUPAC classification. The hysteresis loop at the high relative pressure in the range of 0.5 to 0.9 indicated the existence of micromesoposity. The specific surface area of materials based on BET calculation was 152 m$^2 \cdot$g^{-1}.

DRS-UV-Vis spectra of TiO$_2$/GO (1), Dia-GO (2), and T0.05-100/Dia-GO (3) are presented in Figure 7(a). Bulk TiO$_2$ is considered as an indirect semiconductor [45]. In nanoparticles, the lattice periodicity is lost over a length-scale comparable to the nanoparticle size so the effectiveness of this selection rule breaks down and direct transitions can actually be expected to take place [46, 47]. We used the classical relation near the band-edge optical absorption in a semiconductor to calculate the energy of band-band transition

$$\alpha = \frac{A\left(h\nu - E_g\right)^n}{h\nu}, \qquad (3)$$

where α is the absorption coefficient, E_g is the energy gap, $h\nu$ is the photon energy, and n is equal to 1/2 for direct transitions and 2 for indirect ones. The E_g value can be calculated from the linear plot of $(\alpha h\nu)^{1/n}$ or $(\alpha h\nu)^2$ vs. hν by extrapolating at zero the linear portion near the band-edge. (Figures 7(b) and 7(c)). Both types of plots exhibit the highly linearity with $R^2 = 0.97 - 0.99$ indicating direct or indirect transition that likely occur. The value for
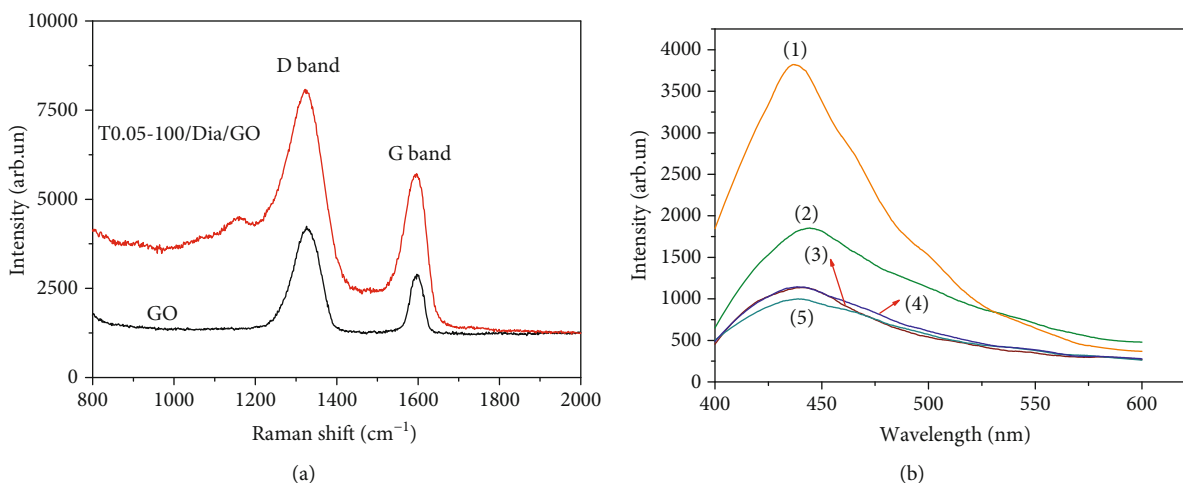
FIGURE 8: (a) Raman spectra of GO and T0.05-100/Dia-GO; (b) photoluminescence (PL) spectra of rutile (1), anatase (2), Dia-GO (3), TiO_2-GO (4), and T0.05-100/Dia-GO (5).

types of band gap energy is listed in Table 2. It is obvious that the value of indirect band energy tends to be lower than direct band energy that is similar to some previous reports [45, 46]. It is found that the indirect band gap energy decreased in the order TiO_2/GO (2.71 eV) > Dia-GO (2.62 eV) > T0.05-100/Dia-GO (2.35 eV) and these TiO_2-based materials exhibit the indirect band gap energy smaller than that of pure TiO_2 (3-3.2 eV) [45–47]. The absorption edge shifts towards a visible region due to the possible interaction of between TiO_2 and modifiers (N and S). This shift is assigned to the generation of intermediate gap energy levels near the valence band of titania. Consequently, narrowing the band gap energy and minimizing the recombination of photoexited electron/hole pairs are considered for the obtained composite T0.05-100/Dia-GO.

Raman spectroscopy is a useful approach for the characterization of the physicochemical properties of graphene-based composites. It is known that in Raman spectroscopy, the G band is assigned to the first-order scattering of the sp^2 C atoms (~1600 cm^{-1}), and the D band is attributed to a breathing mode of k-point photons (~1300 cm^{-1}). At the same time, an increase in I_D/I_G ratio arises from a lower degree of crystallinity in the graphitic structure. Two bands in the Raman spectra of GO and T0.05-100/Dia-GO located at approximately 1300 and 1600 cm^{-1} attributed to the D band and G band, respectively (Figure 8(a)). The I_D/I_G ratio increased from 1.42 for GO to 1.45 for T0.05-100/Dia-GO suggesting a decrease in the size of the in-plane sp^2 domains and the partially ordered crystal structure of graphene oxide. These results provided more evidence for the insert of titania and diazonium salt into graphene oxide.

PL spectra of obtained samples are shown in Figure 8(b). It can be seen that the luminescent intensity of rutile was the highest, followed by anatase, Dia-GO, and TiO_2/GO, and the lowest one belonged to T0.05-100/Dia-GO. It is well known that low PL intensity means

low recombination of electron and holes; then, the opposite would be high PL intensity would increase recombination rate and reduce photocatalytic activity. These results demonstrate that the dispersion of TiO_2 on graphene reduces the recombination of photonic electrons and photogenic holes, which may increase the photocatalytic activity of the material.

Figure 9(a) shows the XPS spectrum of T0.05-100/Dia-GO composite, indicating the presence of the four main elements at 162, 284.6, 529.8, and 458.6 eV corresponding to sulfur (S2p), carbon (C1s), oxygen (O1s), and titanium (Ti2p), respectively. Figure 9(b) shows the XPS Ti2p core level. It can be seen that characteristic peaks are at around 457.6 eV for Ti2p$_{3/2}$ and 463.4 eV for Ti2p$_{1/2}$, indicating a successful loading of Ti on the surface of GO [5, 48]. Figure 9(c) represents the S2p doublet core peak locating at 160.8-169 eV, associated with a sulfonate type [49]. N1s spectrum is shown in Figure 9(d). The binding energy of around 399.6 eV can be assigned to tertiary amine [50]. The C1s spectrum of GO in Figure 9(e) can be deconvoluted into three peaks at 284.6, 286.7, and 288.5 eV, respectively. Two main peaks at 284.6 and 286.7 eV are usually attributed to adventitious carbon and graphitic carbon from GO, and hydroxyl carbon (C-OH), respectively [51]. The other peak at 288.5 eV can be assigned to carboxyl carbon (O-C=O) [51].

3.2. Photocatalytic Performance of TiO_2/Diazonium/GO Composites for MB Degradation in a Visible-Light Region

3.2.1. Leaching Experiment. The kinetics of decolorization of MB in several conditions are shown in Figure 10. It was found that the decolorization of MB was not observed if visible light was irradiated in the absence of T0.05-100/Dia-GO suggesting that MB was stable and did not undergo photolysis. A leaching experiment was also conducted in which the T0.05-100/Dia-GO was filtered by centrifugation after 60 min. of irradiation. The MB
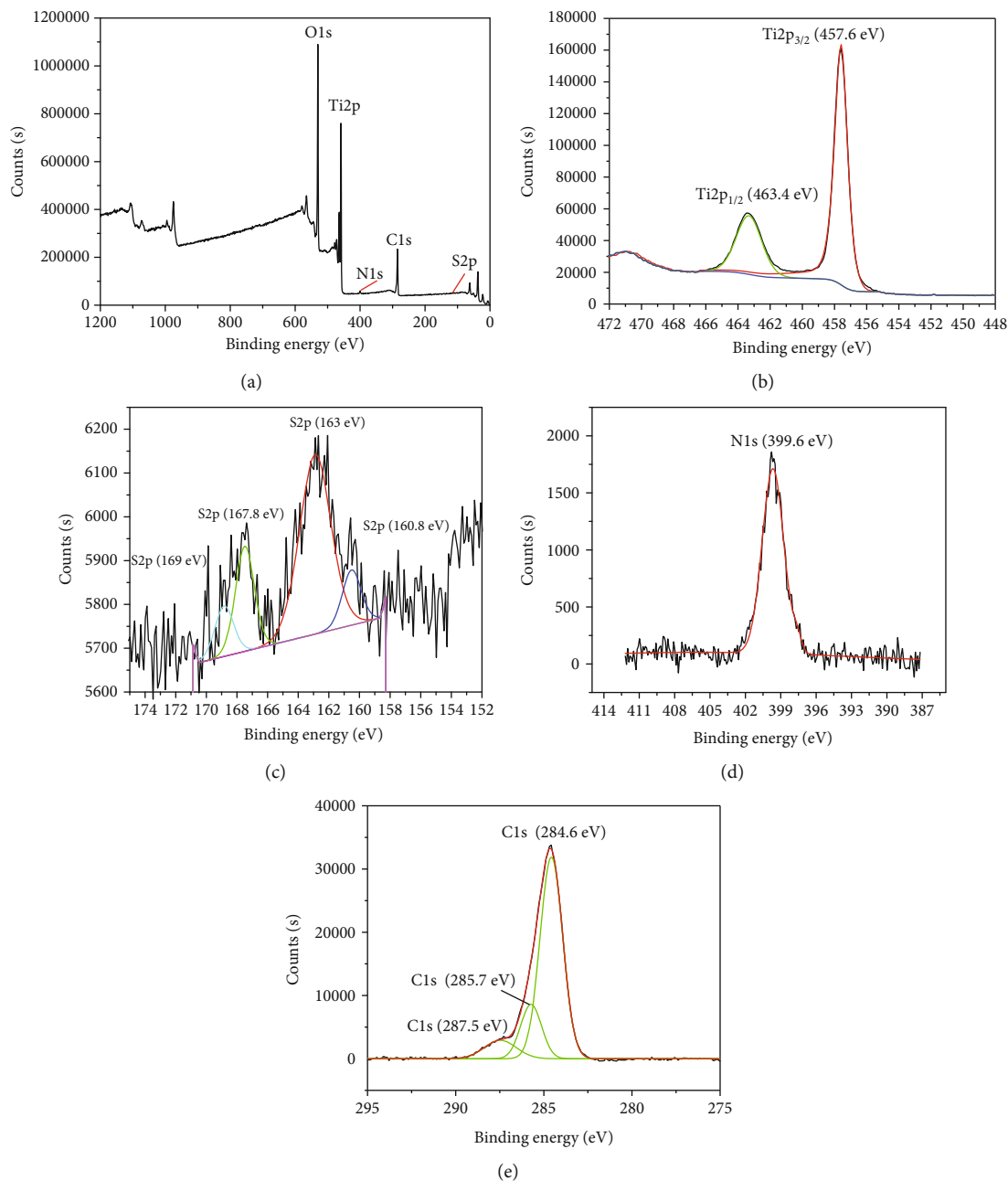
(a)

(b)

(c)

(d)

(e)

FIGURE 9: XPS spectra of T0.05-100/Dia-GO: (a) survey spectrum; (b) Ti2p; (c) S2p; (d) N1s; (e) C1s.

decolorization was quenched even when the light was still irradiated. This indicates that there was no leaching of the active species into the reaction solution from the heterogeneous catalyst. The above experimental results confirmed that T0.05-100/Dia-GO acted as a heterogeneous catalyst in the degradation reaction of MB.

Figure 11(a) presents the adsorption kinetics and photocatalytic decolorization of MB on TiO$_2$/Dia-GO catalyst. This catalyst presented a low adsorption capacity of MB. The adsorption was saturated from 100 min to 120 min depending on the initial MB concentration. In this study, the light illumination was carried out only

when the dark adsorption reached adsorption/desorption equilibrium.

3.2.2. Adsorption Isotherm. The equilibrium adsorption capacity, q_e, can be expressed as follows:

$$q_e = \frac{V \cdot (C_0 - C_e)}{m}, \tag{4}$$

where C_0 and C_e are the MB concentration at initial and equilibrium time (mg·L^{-1}); V is the volume of the MB solution (L); m is the mass of catalyst (g).
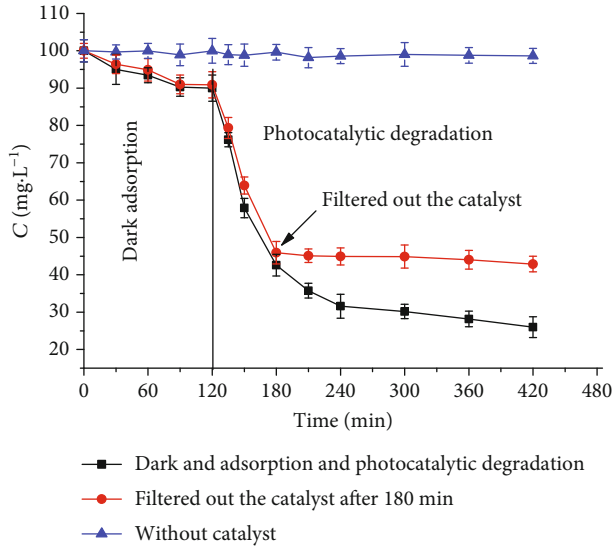
FIGURE 10: Leaching experiment ($V = 500\,\text{mL}$, $C_0 = 100\,\text{mg} \cdot \text{L}^{-1}$; mass of catalyst: 100 mg).

The relationship between C_e and q_e is expressed by the Langmuir isotherm model as equation (5) and the Freundlich model as equation (6):
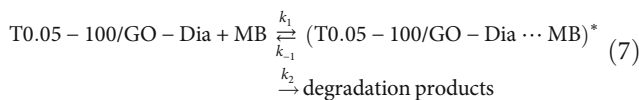
$$q_e = \frac{K_L \cdot q_m \cdot C_e}{1 + K_L \cdot C_e}, \tag{5}$$

$$q_e = K_F \cdot C_e^{1/n}, \tag{6}$$

where q_m is the maximum monolayer adsorption capacity ($\text{mg} \cdot \text{L}^{-1}$); K_L is the Langmuir adsorption equilibrium constant ($\text{mg}^{-1} \cdot \text{L}$); K_F and n are Freundlich parameters.

The calculated parameters can be obtained from nonlinear regression of equations (5) and (6) and are listed in Table 3. A high determination coefficient ($R^2 = 0.99$) for Langmuir model and Freundlich model indicated that the equilibrium data was well fitted in both models. It implies a monolayer adsorption and the existence of heterogeneous surface in the adsorbents.

3.3. Decomposition Kinetics. Based on the Langmuir-Hinshelwood model, the overall reaction could be illustrated as follows:

$$\text{T0.05} - 100/\text{GO} - \text{Dia} + \text{MB} \underset{k_{-1}}{\overset{k_1}{\rightleftarrows}} (\text{T0.05} - 100/\text{GO} - \text{Dia} \cdots \text{MB})^* \overset{k_2}{\to} \text{degradation products} \tag{7}$$

where k_1 and k_{-1} are the forward/back adsorption rate constant, respectively; k_2 is the kinetic rate coefficient of the degradation process.

The law rate is expressed as follows:

$$r = -\frac{dC}{dt} = k_{MLH} \cdot \theta, \tag{8}$$

where C is the dye concentration ($\text{mg} \cdot \text{L}^{-1}$) at time t; k_{MLH} is the kinetic rate coefficient ($\text{mg} \cdot \text{L}^{-1} \cdot \text{min}^{-1}$); θ is the fraction of the surface covered by MB. θ is expressed in the Langmuir model as [37]

$$\theta = \frac{K_L \cdot C}{1 + K_L \cdot C}. \tag{9}$$

Substituting (8) to (6) gives

$$\frac{dC}{dt} = -k_{MLH} \cdot \frac{K_L \cdot C}{1 + K_L \cdot C}. \tag{10}$$

Then,

$$\int \frac{1 + K_L \cdot C}{K_L \cdot C} \cdot dC = -\int k_{MLH} \cdot dt. \tag{11}$$

Integrating equation (11) with the boundary conditions $t \longrightarrow 0$ and $C \longrightarrow C_{0e}$ gives

$$\frac{1}{K_L} \cdot \ln C + C = -k_{MLH} \cdot t + I_0, \tag{12}$$

when $t = 0$, then

$$I_0 = \frac{1}{K_L} \cdot \ln C_{0e} + C_{0e}. \tag{13}$$

Substituting (13) into (12) gives

$$\frac{1}{K_L} \cdot \ln C + C = -k_{MLH} \cdot t + \frac{1}{K_L} \cdot \ln C_{0e} + C_{0e}, \tag{14}$$

where C_{0e} ($\text{mg} \cdot \text{L}^{-1}$) is the equilibrium concentration of adsorbate at time t (min) taken from light illumination.

The plot of the $((1/K) \ln C + C)$ against t gives a straight line with slope k_{MLH} (Figure 11(b)).

For the kinetics of unimolecular reaction on heterogeneous catalyst the Langmuir-Hinshelwood model is widely used. In this study, the Langmuir-Hinshelwood was also applied to calculate the kinetic data for the sake of comparison. This model is as follows:

$$\ln \frac{C_t}{C_0} = -k_{LH} \cdot t, \tag{15}$$

where k_{LH} is the rate constant of the degradation process (min^{-1}); C_0 and C_t are MB initial concentration and concentration at time t ($\text{mg} \cdot \text{L}^{-1}$).

The values of k_{MHL} at different initial MB concentrations for both models are listed in Table 4.

The determination coefficients of the straight lines derived from the modified Langmuir-Hinshelwood model
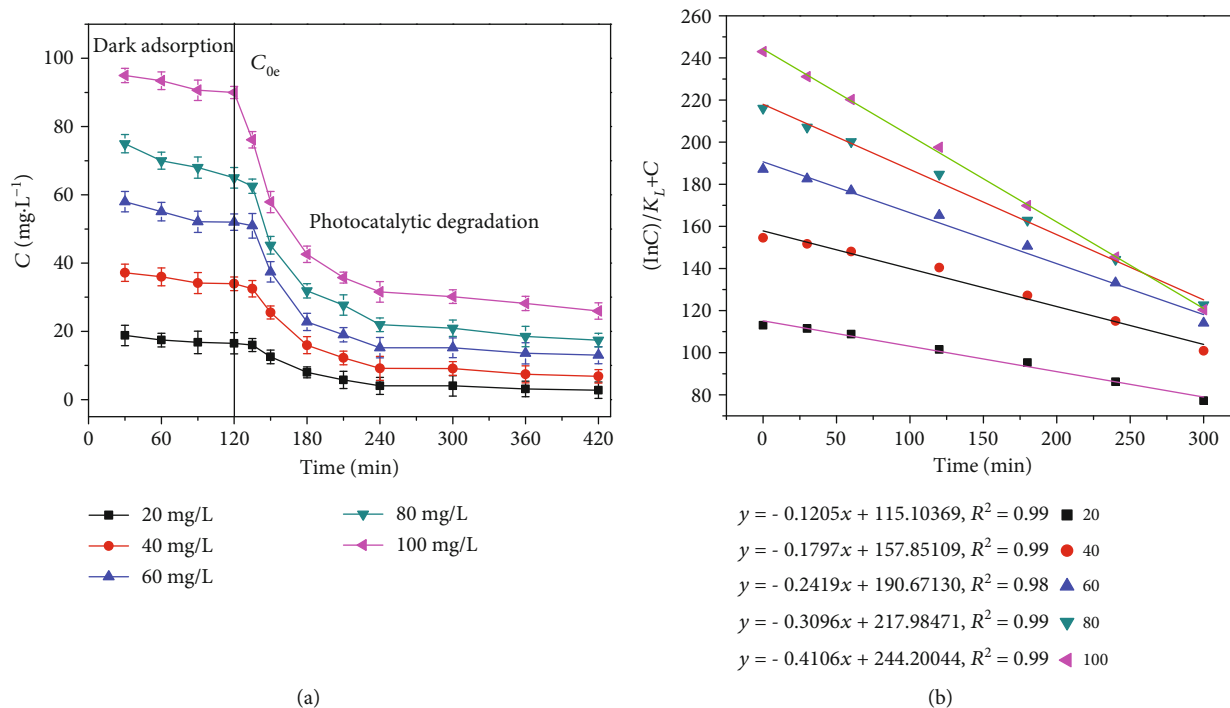
(a)

(b)

FIGURE 11: (a) The adsorption and photodegradation kinetics of MB on T0.05-100/Dia-GO catalyst; (b) the plots of the $(1/K) \ln C + C$ against t different initial MB concentration.

TABLE 3: The parameters of Langmuir and Freundlich model.

	Langmuir model			Freundlich model		
K_L (L·mg^{-1})	q_m (mg·g^{-1})	R^2		K_F	N	R^2
$3.2.10^{-2}$	138.12	0.99		5.837	1.35	0.99

are significantly higher than those of the conventional Langmuir-Hinshelwood model, demonstrating that the proposed modified Langmuir-Hinshelwood model fitted better for the experimental data. The comparison of rate constant calculated by the Langmuir-Hinshelwood model of the present catalyst with published literature is listed in Table 5. The results show that the photocatalytic activity of TiO$_2$/diazonium/GO was relatively high compared with previous reports.

3.3.1. The Proposed Mechanism of MB Degradation. Figure 12 presents the UV-Vis spectra of MB solution at different reaction time.

The MB solution after 30 minutes of photocatalytic oxidation were analyzed by mass spectroscopic LC-MS studies (see Figures S1, 2, 3, 4, and 5). The finding showed that the intermediates with the retention time of 1.88, 1.90, 1.93, 2.13, and 2.21 have m/z, respectively, 91.00259, 153.06585, 139.05020, 103.07536, and 167.08150. The molecular formulae were HOOC-COOH, CH$_3$-CH$_2$-CH$_2$-CH$_2$-COOH, H$_2$N-C$_6$H$_4$-O-N=O, CH$_3$-HN-C$_6$H$_4$-O-N=O, and (CH$_3$)$_2$N-C$_6$H$_4$-O-N=O (see Schemes S1, 2, 3, 4, and 5). These results indicate that phenothiazine structure and benzene were possibly attacked by the hydroxyl or superoxide radicals which were formed with the presence of

photoinduced hole/electron pairs. As the results, they were oxidized and opened the ring to form the intermediates during photocatalytic oxidation. The time dependence of the total organic carbon (TOC) in MB solution during photocatalytic degradation is presented in Figure 12 showing that the TOC value reduced with an increase in irradiation time (13.12 mg·L^{-1} for initial time and 0.67 mg·L^{-1} for 600 min. of photocatalytic degradation). TOC reduced to 95% after 600 minutes which implied that almost all MB is mineralized.

It is well known that the mechanism of photocatalytic reaction in the intermediate phase involves the formation of free radicals, the photoluminescent electrons, and the clear optical holes [60]. In order to understand the mechanism of the reaction, the effect of some quenchers during the catalyst degradation of MB was investigated. In this work, we used benzoquinone (BQ) as a quenching agent for ˙O^{-2}, ammonium oxalate (AO) as the optical h$^+$ hole scavenger, *tert*-Butanol (TB) to quench ˙OH, and dimethyl sulfoxide (DMSO) to quench electron, e-. The solution was quenched with an initial concentration of quencher of 1 mM, for an initial TB concentration of 10 mM. The results are presented in Figure 13.

The research results showed that the presence of a quencher reduced the optical decomposition efficiency of MB compared to the nonquenching system (WQ). The most obvious effect was DMSO where the degradation efficiency only decreased to 18%, followed by AO with a decrease to 37% and then BQ with a drop in the efficiency to 42%. Meanwhile, TB scavenger did not show significant effect on the degradation efficiency. From the contents discussed above, it can be concluded that the original

TABLE 4: The value of k_{MLH} and k_{LH} at different initial MB concentration over T0.05-100/Dia-GO.

| Concentration (mg·L^{-1})	Modified Langmuir-Hinshelwood model		Langmuir-Hinshelwood model	
	k_{MLH} (mg·L^{-1}·min^{-1})	R^2	k_{LH} (min^{-1})	R^2
20	0.121	0.99	0.160	0.98
40	0.180	0.99	0.019	0.97
60	0.242	0.99	0.207	9.96
80	0.310	1	0.235	0.97
100	0.411	1	0.289	0.98

TABLE 5: Comparison of rate constant of the present catalyst with published literature.

Catalyst	BET-specific surface area (m^2·g^{-1})	Light source (nm, powder)	C_0 (mg·L^{-1})/volume (mL)/$m_{catalyst}$ (mg)	k_{LH} (min^{-1})	References
ZnO	8.21	UV, 20 W	10/100/50	0.022	[52]
ZnO/graphene oxide	31.58	UV, 20 W	10/100/50	0.098	[52]
Pristine TiO$_2$ (P25)	—	254, 11 W	10/100/50	0.009	[53]
Graphene-like carbon/TiO$_2$	—	254, 11 W	10/100/50	0.248	[53]
Pristine TiO$_2$ (P25)	51	≤370, 18 W	9.60/100/50	0.050	[54]
Sm-TiO$_2$	46	370, 18 W	9.60/100/50	0.030	[54]
Ce-TiO$_2$	46	370, 18 W	9.60/100/50	0.025	[55]
TiO$_2$	50	340, 125 W	23/2750/375	0.025	[56]
CdS	111.2	>420, 500w	25/200/80	0.008	[56]
g-C$_3$N$_4$	9.8	>420, 500w	25/200/80	0.004	[56]
g-C$_3$N$_4$-CdS	166.5	>420, 500w	25/200/80	0.012	[56]
Ag/ZnO	—	>570, (high pressure sodium lamp)	5/-/150	0.005	[57]
Ta-ZnO	36	>420, 300	10/50/50	0.040	[58]
Eu-TiO$_2$	—	(400-800 nm), 60 W, halogen lamp	3.19/100/100	0.008	[59]
TiO$_2$/diazonium/GO	151.4	75 W - 220 V	20/100/100	0.160	The present work
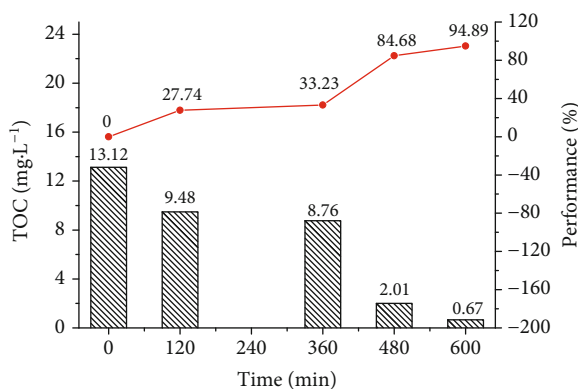
FIGURE 12: TOC of MB solution in the photocatalytic degradation ($V = 100$ mL; $C_0 = 100$ ppm; $m_{catalyst} = 100$ mg; reaction time is 30 min).

superoxide anion ($^{·}O^{-2}$), photogenic electrons, e-, and photogenic holes, h$^+$, all contribute to the MB decomposition process. Among the three determinants of the photocatalytic process performance of the study material are photoluminescence and photonic hole, the most important is the presence of photogenic electrons.
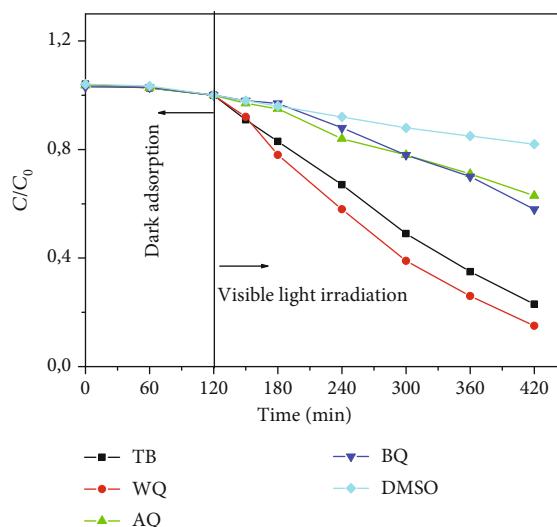
FIGURE 13: Photocatalytic degradation of MB by T0.05-100/Dia-GO using quencher AO, BQ, TB, DMSO, and without quencher (WQ) under visible light irradiation for 420 min (condition: concentration of MB, $C_0 = 100$ ppm; $V = 100$ mL).
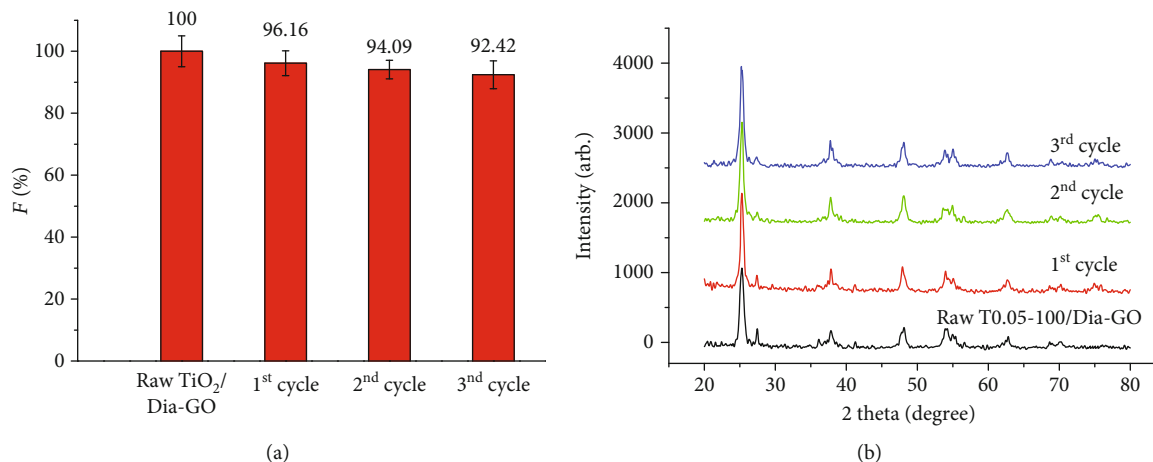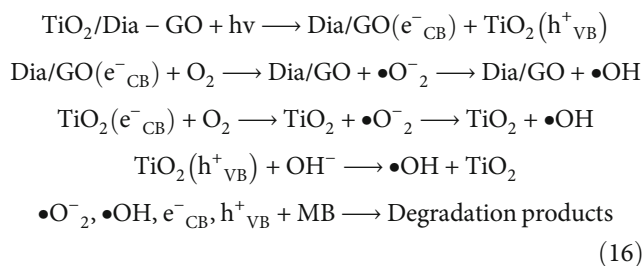
FIGURE 14: (a) Photocatalytic degradation efficiency of used catalysts; (b) XRD patterns of T0.05-100/Dia-GO after three cycles of catalysis (V = 1000 mL, C_0 = 10 ppm, $m_{catalyst}$ = 500 mg; adsorption time is 120 min; light-illumination time is 120 min).

Proposed mechanism for the degradation of MB under visible light-illumination in the presence of the TiO$_2$/Dia-GO photocatalyst is as follows:

$$TiO_2/Dia - GO + hv \longrightarrow Dia/GO(e^-_{CB}) + TiO_2(h^+_{VB})$$

$$Dia/GO(e^-_{CB}) + O_2 \longrightarrow Dia/GO + \bullet O^-_2 \longrightarrow Dia/GO + \bullet OH$$

$$TiO_2(e^-_{CB}) + O_2 \longrightarrow TiO_2 + \bullet O^-_2 \longrightarrow TiO_2 + \bullet OH$$

$$TiO_2(h^+_{VB}) + OH^- \longrightarrow \bullet OH + TiO_2$$

$$\bullet O^-_2, \bullet OH, e^-_{CB}, h^+_{VB} + MB \longrightarrow Degradation\ products$$

$$(16)$$

3.3.2. Recyclability. The T0.05-100/Dia-GO catalyst was reused for several times. After each run, it was separated by centrifugation, then washed with water and ethanol for three times to remove any dye residual, and finally dried at 120˚C for 15 h. The photocatalytic degradation efficiency of T0.05-100/Dia-GO decreased from 100% to 92.72% after three cycles (Figure 14(a)). The XRD patterns of the recycled TiO$_2$/Dia-GO samples stayed unaltered; therefore, it can be inferred that TiO$_2$/Dia-GO remained stable during photocatalytic degradation reactions (Figure 14(b)).

In addition, the obtained catalyst manifested excellent photocatalytic degradation of several other dyes, including phenol, methyl orange, and Congo red. As can be seen in Figure 15, T0.05-100/Dia-GO composite exhibited superior visible-light-responsive photocatalytic degradation of MB compared with single TiO$_2$ and TiO$_2$/GO.

4. Conclusion

The synthesis of TiO$_2$/diazonium/GO and an application to MB photocatalytic degradation in a visible region have been studied. Rutile or anatase phase in TiO$_2$/diazonium/GO composites can be controlled by adjusting the amount of TiCl$_4$ in the reaction mixture or ethanol/water ratio for hydrolysis. TiO$_2$/diazonium/GO with *ac.* 70% anatase in titania phase provided the highest MB degradation efficiency.
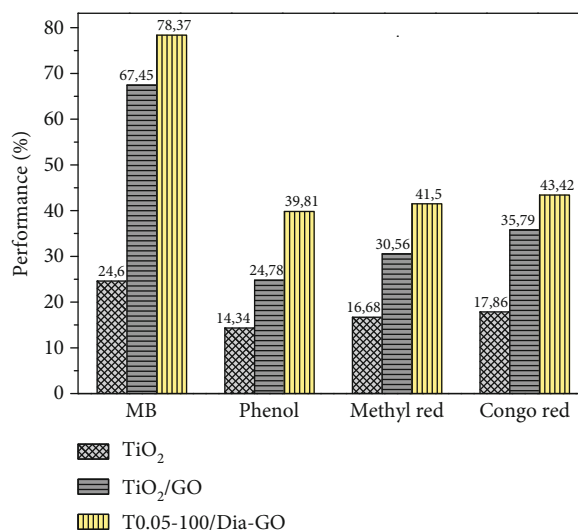

FIGURE 15: Visible-light-driven photocatalytic degradation of several dyes over TiO$_2$, TiO$_2$/GO and T0.05-100/Dia-GO composite (condition: concentration of dyes = 100 mg/L; V = 100 mL; $m_{catalyst}$ = 100 mg; illumination time is 300 min).

The photocatalytic oxidation exhibited a complete decomposition of MB by the cleavage and oxidation of one or more of the methyl substituents on the amine groups. We have proposed a kinetic model by the combination of classical Langmuir-Hinshelwood kinetic model and Langmuir isotherm model. The experimental data fit well the proposed model. In addition, TiO$_2$/diazonium/GO composite can catalyze for photodegradation of several dyes such as phenol, Congo red, and methyl red. The present catalyst with its stability and recyclable advantages is promising for application in the treatment of dye wastes.

Data Availability

The data used to support the findings of this study are available from the corresponding author upon request.

Conflicts of Interest

The authors declare that they have no conflicts of interest.

Acknowledgments

Supplementary Materials

The liquid chromatography-mass spectroscopy (LC-MS) analysis of the methylene blue (MB) solution recorded after 30 min of photocatalytic treatment is presented in Figure 1–5S. This experimental data implies that at the end of 30 min irradiation, the reaction solution was significantly decolorized or degraded. This is evident by the decrease in the MB peak intensity and the appearance of new peaks detected at lower retention times which correspond to new photocatalytic products of the dye. The finding showed that the intermediates with the retention time of 1.88, 1.90, 1.93, 2.13, and 2.21 have m/z, respectively, 91.00259, 153.06585, 139.05020, 103.07536, and 167.08150. The molecular formulae were HOOC-COOH, CH3-HN-C6H4-O-N=O, H2N-C6H4-O-N=O, CH3-CH2-CH2-CH2-COOH, and (CH3)2N-C6H4-O-N=O (Schemes 1, 2, 3, 4, and 5S). The proposed mass spectrometry fragmentation mechanism for the compound at retention time of 1.88 min is shown in Scheme 1S. This compound has a formula that could be HOOC-COOH. The proposed mass spectrometry fragmentation mechanisms for the compound at retention time of 1.9 min. The possible formula is CH3-HN-C6H4-O-N=O. The proposed mass spectrometry fragmentation mechanisms for the compound at retention time of 1.93 min is shown in Scheme 3S. The possible formula of this compound is H2N-C6H4-O-N=O. The proposed mass spectrometry fragmentation mechanisms for the compound at retention time of 2.13 min is shown in Scheme 4S. Its formula could be CH3-CH2-CH2-CH2-COOH. The proposed mass spectrometry fragmentation mechanisms for the compound at retention time of 2.21 min. is shown in Scheme 5S. This possible formula is (CH3)2NC6H4-O-N=O. (Supplementary Materials)

References

[1] E. Fazio, P. Calandra, V. T. Liveri, N. Santo, and S. Trusso, "Synthesis and physico-chemical characterization of Au/TiO$_2$ nanostructures formed by novel "cold" and "hot" nanosoldering of Au and TiO$_2$ nanoparticles dispersed in water," *Colloids and Surfaces A: Physicochemical and Engineering Aspects*, vol. 392, no. 1, pp. 171–177, 2011.

[2] O. M. Alfano, D. Bahnemann, A. E. Cassano, R. Dillert, and R. Goslich, "Photocatalysis in water environments using artificial and solar light," *Catalysis Today*, vol. 58, no. 2-3, pp. 199–230, 2000.

[3] D. Choi, D. Wang, V. V. Viswanathan et al., "Li-ion batteries from LiFePO$_4$ cathode and anatase/graphene composite anode for stationary energy storage," *Electrochemistry Communications*, vol. 12, no. 3, pp. 378–381, 2010.

[4] Z. Liu, X. Zhang, S. Nishimoto, T. Murakami, and A. Fujishima, "Efficient photocatalytic degradation of gaseous acetaldehyde by highly ordered TiO$_2$ nanotube arrays," *Environmental Science & Technology*, vol. 42, no. 22, pp. 8547–8551, 2008.

[5] L. M. Sikhwivhilu, S. Sinha Ray, and N. J. Coville, "Influence of bases on hydrothermal synthesis of titanate nanostructures," *Applied Physics A*, vol. 94, no. 4, pp. 963–973, 2009.

[6] J. Zhang, P. Zhou, J. Liu, and J. Yu, "New understanding of the difference of photocatalytic activity among anatase, rutile and brookite TiO$_2$," *Physical Chemistry Chemical Physics*, vol. 16, no. 38, pp. 20382–20386, 2014.

[7] D. O. Scanlon, C. W. Dunnill, J. Buckeridge et al., "Band alignment of rutile and anatase TiO$_2$," *Nature materials*, vol. 12, no. 9, pp. 798–801, 2013.

[8] X. Shu, Z. An, L. Wang, and J. He, "Metal oxide-sensitized TiO$_2$ and TiO2–xNx with efficient charge transport conduits," *Chemical Communications*, no. 39, pp. 5901–5903, 2009.

[9] T. Tatsuma, S. Saitoh, P. Ngaotrakanwiwat, Y. Ohko, and A. Fujishima, "Energy storage of TiO2–WO3Photocatalysis systems in the gas phase," *Langmuir*, vol. 18, no. 21, pp. 7777–7779, 2002.

[10] C. He, Y. Xiong, and X. Zhu, "A novel method for improving photocatalytic activity of TiO$_2$ film: the combination of Ag deposition with application of external electric field," *Thin Solid Films*, vol. 422, no. 1-2, pp. 235–238, 2002.

[11] I. Bannat, K. Wessels, T. Oekermann, J. Rathousky, D. Bahnemann, and M. Wark, "Improving the photocatalytic performance of mesoporous titania films by modification with gold nanostructures," *Chemistry of Materials*, vol. 21, no. 8, pp. 1645–1653, 2009.

[12] Y. Yu, J. C. Yu, J. G. Yu et al., "Enhancement of photocatalytic activity of mesoporous TiO$_2$ by using carbon nanotubes," *Applied Catalysis A: General*, vol. 289, no. 2, pp. 186–196, 2005.

[13] H. Wang, X. Quan, H. Yu, and S. Chen, "Fabrication of a TiO$_2$/carbon nanowall heterojunction and its photocatalytic ability," *Carbon*, vol. 46, no. 8, pp. 1126–1132, 2008.

[14] L. Zhi and K. Müllen, "A bottom-up approach from molecular nanographenes to unconventional carbon materials," *Journal of Materials Chemistry*, vol. 18, no. 13, pp. 1472–1484, 2008.

[15] R. Nair, P. Blake, A. N. Grigorenko et al., "Fine structure constant defines visual transparency of graphene," *Science*, vol. 320, no. 5881, pp. 1308–1308, 2008.

[16] S. Sun, L. Gao, and Y. Liu, "Enhanced dye-sensitized solar cell using graphene-TiO$_2$ photoanode prepared by heterogeneous coagulation," *Applied physics letters*, vol. 96, no. 8, p. 083113, 2010.

[17] Y. Li, L. Tang, and J. Li, "Preparation and electrochemical performance for methanol oxidation of Pt/graphene nanocomposites," *Electrochemistry Communications*, vol. 11, no. 4, pp. 846–849, 2009.

[18] C. Nethravathi, T. Nisha, N. Ravishankar, C. Shivakumara, and M. Rajamathi, "Graphene-nanocrystalline metal sulphide composites produced by a one-pot reaction starting

from graphite oxide," *Carbon*, vol. 47, no. 8, pp. 2054–2059, 2009.

[19] L. Liu, S. Ryu, M. R. Tomasik et al., "Graphene oxidation: thickness-dependent etching and strong chemical doping," *Nano Letters*, vol. 8, no. 7, pp. 1965–1970, 2008.

[20] D. W. Boukhvalov and M. I. Katsnelson, "Modeling of graphite oxide," *Journal of the American Chemical Society*, vol. 130, no. 32, pp. 10697–10701, 2008.

[21] X. Wu, M. Sprinkle, X. Li, F. Ming, C. Berger, and W. A. de Heer, "Epitaxial-graphene/graphene-oxide junction: an essential step towards epitaxial graphene electronics," *Physical review letters*, vol. 101, no. 2, p. 026801, 2008.

[22] C. Chen, W. Cai, M. Long et al., "Synthesis of visible-light responsive graphene oxide/TiO(2) composites with p/n heterojunction," *ACS Nano*, vol. 4, no. 11, pp. 6425–6432, 2010.

[23] J. Liu, H. Bai, Y. Wang, Z. Liu, X. Zhang, and D. D. Sun, "Self-assembling TiO_2 nanorods on large graphene oxide sheets at a two-phase interface and their anti-recombination in photocatalytic applications," *Advanced Functional Materials*, vol. 20, no. 23, pp. 4175–4181, 2010.

[24] G. Williams, B. Seger, and P. V. Kamat, "TiO_2-graphene nanocomposites. UV-assisted photocatalytic reduction of graphene oxide," *ACS Nano*, vol. 2, no. 7, pp. 1487–1491, 2008.

[25] H.-L. Ma, Y. Zhang, Q.-H. Hu, D. Yan, Z.-Z. Yu, and M. Zhai, "Chemical reduction and removal of Cr (VI) from acidic aqueous solution by ethylenediamine-reduced graphene oxide," *Journal of Materials Chemistry*, vol. 22, no. 13, pp. 5914–5916, 2012.

[26] C. J. Madadrang, H. Y. Kim, G. Gao et al., "Adsorption behavior of EDTA-graphene oxide for Pb (II) removal," *ACS Applied Materials & Interfaces*, vol. 4, no. 3, pp. 1186–1193, 2012.

[27] Y. Si and E. T. Samulski, "Synthesis of water soluble graphene," *Nano Letters*, vol. 8, no. 6, pp. 1679–1682, 2008.

[28] W. S. Hummers Jr. and R. E. Offeman, "Preparation of graphitic oxide," *Journal of the American Chemical Society*, vol. 80, no. 6, pp. 1339–1339, 1958.

[29] W. Wang, J. Yu, Q. Xiang, and B. Cheng, "Enhanced photocatalytic activity of hierarchical macro/mesoporous TiO_2-graphene composites for photodegradation of acetone in air," *Applied Catalysis B: Environmental*, vol. 119-120, pp. 109–116, 2012.

[30] R. A. Spurr and H. Myers, "Quantitative analysis of anatase-rutile mixtures with an X-ray diffractometer," *Analytical Chemistry*, vol. 29, no. 5, pp. 760–762, 1957.

[31] V. S. Channu, R. Bobba, and R. Holze, "Graphite and graphene oxide electrodes for lithium ion batteries," *Colloids and Surfaces A: Physicochemical and Engineering Aspects*, vol. 436, pp. 245–251, 2013.

[32] L. Feng, M. Cao, X. Ma, Y. Zhu, and C. Hu, "Superparamagnetic high-surface-area Fe_3O_4 nanoparticles as adsorbents for arsenic removal," *Journal of Hazardous Materials*, vol. 217-218, pp. 439–446, 2012.

[33] N. T. V. Hoan, N. T. A. Thu, H. Van Duc, N. D. Cuong, D. Q. Khieu, and V. Vo, "Fe_3O_4/Reduced Graphene Oxide Nanocomposite: Synthesis and Its Application for Toxic Metal Ion Removal," *Journal of Chemistry*, vol. 2016, Article ID 2418172, 10 pages, 2016.

[34] L. Guo, P. Ye, J. Wang, F. Fu, and Z. Wu, "Three-dimensional Fe_3O_4-graphene macroscopic composites for arsenic and arsenate removal," *Journal of Hazardous Materials*, vol. 298, pp. 28–35, 2015.

[35] P. S. Teo, H. N. Lim, N. M. Huang, C. H. Chia, and I. Harrison, "Room temperature in situ chemical synthesis of Fe_3O_4/graphene," *Ceramics International*, vol. 38, no. 8, pp. 6411–6416, 2012.

[36] E. E. Tkalya, M. Ghislandi, G. de With, and C. E. Koning, "The use of surfactants for dispersing carbon nanotubes and graphene to make conductive nanocomposites," *Current Opinion in Colloid & Interface Science*, vol. 17, no. 4, pp. 225–232, 2012.

[37] Q. Li, B. Guo, J. Yu et al., "Highly efficient visible-light-driven photocatalytic hydrogen production of CdS-cluster-decorated graphene nanosheets," *Journal of the American Chemical Society*, vol. 133, no. 28, pp. 10878–10884, 2011.

[38] J. Shen, T. Li, Y. Long, M. Shi, N. Li, and M. Ye, "One-step solid state preparation of reduced graphene oxide," *Carbon*, vol. 50, no. 6, pp. 2134–2140, 2012.

[39] Y. Xu, H. Bai, G. Lu, C. Li, and G. Shi, "Flexible graphene films via the filtration of water-soluble noncovalent functionalized graphene sheets," *Journal of the American Chemical Society*, vol. 130, no. 18, pp. 5856-5857, 2008.

[40] Y. Niu, M. Xing, B. Tian, and J. Zhang, "Improving the visible light photocatalytic activity of nano-sized titanium dioxide via the synergistic effects between sulfur doping and sulfation," *Applied Catalysis B: Environmental*, vol. 115-116, pp. 253–260, 2012.

[41] E. Doustkhah and S. Rostamnia, "Covalently bonded sulfonic acid magnetic graphene oxide: Fe3O4@ GO-Pr-SO3H as a powerful hybrid catalyst for synthesis of indazolophthalazine-triones," *Journal of Colloid and Interface Science*, vol. 478, pp. 280–287, 2016.

[42] S. Hosseini and A. Amoozadeh, "Nano-TiO_2-P25-SO$_3$H as a new and robust photo-catalyst: the acceleration effect of selective oxidation of aromatic alcohols to aldehydes under blue LED irradiation," *Journal of Photochemistry and Photobiology A: Chemistry*, vol. 364, pp. 516–523, 2018.

[43] M. Abbas, B. P. Rao, V. Reddy, and C. Kim, "Fe_3O_4/TiO_2 core/shell nanocubes: single-batch surfactantless synthesis, characterization and efficient catalysts for methylene blue degradation," *Ceramics International*, vol. 40, no. 7, pp. 11177–11186, 2014.

[44] J. Schneider, M. Matsuoka, M. Takeuchi et al., "Understanding TiO_2 photocatalysis: mechanisms and materials," *Chemical Reviews*, vol. 114, no. 19, pp. 9919–9986, 2014.

[45] P. Calandra, D. Lombardo, A. Pistone, V. Turco Liveri, and S. Trusso, "Structural and optical properties of novel surfactant-coated Yb@ TiO_2 nanoparticles," *Journal of Nanoparticle Research*, vol. 13, no. 11, pp. 5833–5839, 2011.

[46] N. Serpone, D. Lawless, and R. Khairutdinov, "Size effects on the photophysical properties of colloidal anatase TiO_2 particles: size quantization versus direct transitions in this indirect semiconductor?," *The Journal of Physical Chemistry*, vol. 99, no. 45, pp. 16646–16654, 1995.

[47] P. Calandra, A. Ruggirello, A. Pistone, and V. Turco Liveri, "Structural and optical properties of novel surfactant coated TiO_2–Ag based nanoparticles," *Journal of Cluster Science*, vol. 21, no. 4, pp. 767–778, 2010.

[48] W. Kim, T. Tachikawa, G. H. Moon, T. Majima, and W. Choi, "Molecular-level understanding of the photocatalytic activity difference between anatase and rutile nanoparticles," *Angewandte Chemie International Edition*, vol. 53, no. 51, pp. 14036–14041, 2014.

[49] S. Fleutot, H. Martinez, J. C. Dupin et al., "Experimental (X-ray photoelectron spectroscopy) and theoretical studies of benzene based organics intercalated into layered double hydroxide," *Solid State Sciences*, vol. 13, no. 9, pp. 1676–1686, 2011.

[50] G. Forget, L. Latxague, V. Heroguez, C. Labrugere, and M. C. Durrieu, "RGD nanodomains grafting onto titanium surface," in *2007 29th Annual International Conference of the IEEE Engineering in Medicine and Biology Society*, pp. 5107–5110, Lyon, France, 22-26 Aug. 2007.

[51] F. T. Johra, J.-W. Lee, and W.-G. Jung, "Facile and safe graphene preparation on solution based platform," *Journal of Industrial and Engineering Chemistry*, vol. 20, no. 5, pp. 2883–2887, 2014.

[52] H. Fan, X. Zhao, J. Yang et al., "ZnO-graphene composite for photocatalytic degradation of methylene blue dye," *Catalysis Communications*, vol. 29, pp. 29–34, 2012.

[53] Y. Wang, R. Shi, J. Lin, and Y. Zhu, "Significant photocatalytic enhancement in methylene blue degradation of TiO_2 photocatalysts via graphene-like carbon in situ hybridization," *Applied Catalysis B: Environmental*, vol. 100, no. 1-2, pp. 179–183, 2010.

[54] P. Du, A. Bueno-López, M. Verbaas et al., "The effect of surface OH-population on the photocatalytic activity of rare earth-doped $P25-TiO_2$ in methylene blue degradation," *Journal of Catalysis*, vol. 260, no. 1, pp. 75–80, 2008.

[55] L. T. T. Tuyen, D. A. Quang, T. T. Tam Toan et al., "Synthesis of CeO_2/TiO_2 nanotubes and heterogeneous photocatalytic degradation of methylene blue," *Journal of Environmental Chemical Engineering*, vol. 6, no. 5, pp. 5999–6011, 2018.

[56] A. Houas, H. Lachheb, M. Ksibi, E. Elaloui, C. Guillard, and J.-M. Herrmann, "Photocatalytic degradation pathway of methylene blue in water," *Applied Catalysis B: Environmental*, vol. 31, no. 2, pp. 145–157, 2001.

[57] T.-J. Whang, M.-T. Hsieh, and H.-H. Chen, "Visible-light photocatalytic degradation of methylene blue with laser-induced Ag/ZnO nanoparticles," *Applied Surface Science*, vol. 258, no. 7, pp. 2796–2801, 2012.

[58] J. Z. Kong, A. D. Li, X. Y. Li et al., "Photo-degradation of methylene blue using Ta-doped ZnO nanoparticle," *Journal of Solid State Chemistry*, vol. 183, no. 6, pp. 1359–1364, 2010.

[59] D. Caschera, F. Federici, T. de Caro et al., "Fabrication of Eu-TiO_2 NCs functionalized cotton textile as a multifunctional photocatalyst for dye pollutants degradation," *Applied Surface Science*, vol. 427, pp. 81–91, 2018.

[60] W. Wang, K. Xiao, L. Zhu, Y. Yin, and Z. Wang, "Graphene oxide supported titanium dioxide & ferroferric oxide hybrid, a magnetically separable photocatalyst with enhanced photocatalytic activity for tetracycline hydrochloride degradation," *RSC Advances*, vol. 7, no. 34, pp. 21287–21297, 2017.

The Scientific
World Journal

Journal of
Applied Chemistry

Journal of
Nanomaterials

Scientifica

International Journal of
Polymer Science

Advances in
Chemistry

Advances in
Physical Chemistry

International Journal of
Analytical Chemistry

Hindawi

Submit your manuscripts at
www.hindawi.com

Advances in
Condensed Matter Physics

Journal of
Chemistry

International Journal of
Biomaterials

Advances in
High Energy Physics

Journal of
Engineering

Journal of
Nanotechnology

International Journal of
Corrosion

Journal of
Materials

BioMed
Research International

Advances in
Tribology

Advances in
Materials Science and Engineering